Striped, Ellipsoidal Particles by Controlled Assembly of Diblock Copolymers

Se Gyu Jang,[†,∇] Debra J. Audus,[†,‡] Daniel Klinger,[†] Daniel V. Krogstad,[†,§] Bumjoon J. Kim,[⊥] Alexandre Cameron,[†] Sang-Woo Kim,[†] Kris T. Delaney,[†] Su-Mi Hur,[†] Kato L. Killops,[#] Glenn H. Fredrickson,*[,†,‡,§] Edward J. Kramer,*[,†,‡,§] and Craig J. Hawker*[,†,§,‖]

[†]Materials Research Laboratory, [‡]Department of Chemical Engineering, [§]Department of Materials, and [‖]Department of Chemistry and Biochemistry, University of California, Santa Barbara, California 93106, United States

[⊥]Department of Chemical and Biomolecular Engineering, Korea Advanced Institute of Science and Technology, Daehon 305-701, Republic of Korea

[#]Edgewood Chemical Biological Center, U.S. Army Research, Development, and Engineering Command, Aberdeen Proving Ground, Maryland 21010, United States

S *Supporting Information*

ABSTRACT: Control of interfacial interactions leads to a dramatic change in shape and morphology for particles based on poly(styrene-*b*-2-vinylpyridine) diblock copolymers. Key to these changes is the addition of Au-based surfactant nano-particles (SNPs) which are adsorbed at the interface between block copolymer-containing emulsion droplets and the surrounding amphiphilic surfactant to afford asymmetric, ellipsoid particles. The mechanism of formation for these novel nanostructures was investigated by systematically varying the volume fraction of SNPs, with the results showing the critical nature that the segregation of SNPs to specific interfaces plays in controlling structure. A theoretical description of the system allows the size distribution and aspect ratio of the asymmetric block copolymer colloidal particles to be correlated with the experimental results.

Surfactant Nanoparticles
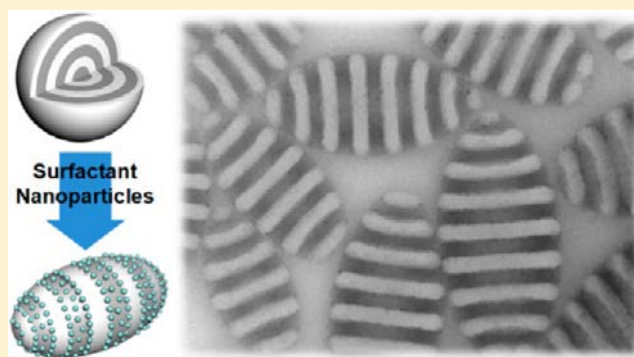
INTRODUCTION

One of the grand challenges in the broad materials field is to control the self-assembly of multicomponent systems for the preparation of asymmetric or low-symmetry structures on a submicrometer length scale. In addressing this opportunity, the coassembly of inorganic nanoparticles and block copolymers has been intensively studied for the creation of multifunctional hybrid materials where the unique physical/chemical properties of nanoparticles are coupled with self-assembled, block copolymer nanostructures.[1−5] In bulk systems, recent reports have demonstrated that precise control of nanoparticle segregation either into the A (or B) domain or at the interface of A-*b*-B block copolymers could be achieved by careful control of nanoparticle surface properties.[6−24] This addition of inorganic nanoparticles to block copolymer domains not only adds the functionality of nanoparticles to the ordered block copolymer structure but can also induce useful morphological transitions. For example, nanoparticle segregation to the A domain results in an increase in volume fraction and associated morphological transitions that are comparable to those induced by the addition of A homopolymers.[5,20,22,25] Alternatively, if the nanoparticles segregate strongly to the A/B interface, transition of an A-*b*-B diblock copolymer from a lamellar morphology to a

disordered bicontinuous morphology can be achieved.[15,16,26−28] For poly(styrene-*b*-2-vinylpyridine) (PS-*b*-P2VP) materials, precise control of an attractive secondary interaction between Au-based nanoparticles and the P2VP block was found to be a key factor in driving segregation of the nanoparticles to interfaces with high enough volume fraction to induce morphology transitions.[27,28]

In analogy with the above bulk studies, the utility of using interfacially active nanoparticles has also been demonstrated by controlling the orientation of block copolymer domains in thin films. Theoretical calculations using self-consistent mean field theory (SCFT) and density functional theory (DFT) reveal that nanoparticles with neutral surface interactions balance the interfacial energies between the substrate and a symmetric diblock copolymer by segregation to the substrate.[29] This theoretical prediction has been experimentally verified by the observation of induced perpendicular orientation of poly-(styrene-*b*-methyl methacrylate) (PS-*b*-PMMA) films by addition of Au nanoparticles with polar cross-linked shells[30] or hydrophilic poly(ethylene oxide) (PEO) ligands.[31] The Au

nanoparticles that are preferentially segregated near the substrate or the polymer/air interface act like a neutral layer to allow PS and PMMA domains to evenly wet the substrate or air interfaces. These instances of morphological transition and orientation control of ordered block copolymer microdomains by addition of nanoparticles are practically useful as well as theoretically interesting.

To date, the effect of nanoparticles on phase separation has been limited to either bulk or thin-film samples,[32] which is unfortunate since there is a growing interest in the unique morphologies obtained through self-assembly of block copolymers in confined geometries.[33−40] Yabu et al. and Higuchi et al. have studied the morphology of block copolymer systems created by the slow evaporation of a good solvent from swollen colloidal particles, which allows for the capture of thermodynamically unstable or metastable morphologies.[41−47] For example, a kinetically trapped morphology with axially stacked lamellae of poly(styrene-b-isoprene) (PS-b-PI) has been observed, with this nanostructure undergoing a transition to a thermodynamically more stable, onion-shaped morphology on thermal annealing.[42] A critical parameter in determining the morphology within this confined geometry is the interfacial interaction between block copolymers and the surrounding media. Compared to thin films or the bulk case, these interactions are magnified by the high surface area of colloidal particles relative to their volume. Recently, Yang et al. demonstrated transition of poly(styrene-b-butadiene) (PS-b-PB) block copolymer colloidal particle morphologies from onion-like to axially stacked lamellae by using mixed surfactants, short PS-b-PEO and PB-b-PEO block copolymers, which neutralized the interfacial interaction between each block of a PS-b-PB block copolymer and the surrounding wall of an emulsion droplet.[48,49] Such asymmetric particles are generally of significant interest as they allow fundamental insights into the self-assembly of anisotropic colloidal particles[50,51] while also providing novel systems for a variety of applications,[52,53] including drug delivery[54] and shape-dependent modulation of cellular interactions.[55,56] Moreover, this concept also demonstrates that fine-tuning of the interfacial property is a powerful strategy for creating block copolymer colloidal particles with nonconventional shapes and morphologies.

Here, we report a novel strategy involving the combination of confined geometry templating with tunable interfacial interactions through surfactant nanoparticles (SNPs) for the formation of asymmetric nanostructures (Figure 1). In the
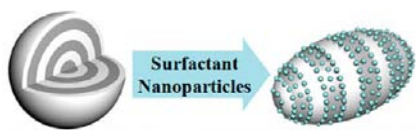

Figure 1. Schematic illustrating the change in shape and morphology of block copolymer particles resulting from the addition of SNPs.

absence of SNPs, slow evaporation of chloroform from emulsion droplets containing PS-b-P2VP diblock copolymers resulted in solid particles with a spherical, radial morphology due to preferential wetting of PS domains on the hydrophobic tail group of the surrounding amphiphilic surfactant (cetyl-trimethylammonium bromide, CTAB). In direct contrast, the addition of SNPs—designed to adsorb at the emulsion/CTAB interface—led to a dramatic change in the internal morphology and overall shape of the block copolymer colloidal particles.

Ellipsoidal block copolymer colloidal particles with axially stacked lamellae of PS-b-P2VP and SNP necklaces decorating the outer surface could be obtained. The role of interfacially active SNPs in the morphology transition and the formation mechanism was systematically studied by varying the volume fraction of SNPs, by investigating the influence of the initial sizes of emulsion droplets, and by tracking the segregation location of the SNPs. Interestingly, the strategies developed for block copolymer systems could also be applied to homopolymer mixtures, leading to a facile synthesis method for "Janus" colloidal particles.

RESULTS AND DISCUSSION

Block copolymer colloidal particles were produced from a chloroform-in-water emulsion by initially dissolving symmetric PS-b-P2VP block copolymer (199 kg/mol) in chloroform (1 wt %) with or without SNPs (Scheme 1; the structural information

Scheme 1. Schematic Illustrating the Synthetic Procedure of Block Copolymer Colloidal Particles from a Chloroform-in-Water Emulsion
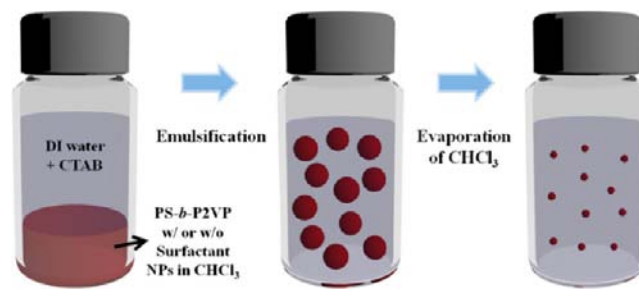
and interfacial activity for the SNPs will be described below). The chloroform solutions were then mixed with deionized water containing 0.1 wt % amphiphilic cationic surfactant (CTAB), emulsified by ultrasonication, and the chloroform in the emulsion droplets was allowed to slowly evaporate through the water phase, leading to glassy block copolymer colloidal particles dispersed in water. It should be noted that adsorption of SNPs to the emulsion/surfactant interface is highly affected by interfacial interaction between the SNPs and surfactant. No adsorption of SNPs at the emulsion/surfactant interface and corresponding morphology transition from radial lamellar (RL) to axially stacked lamellar (ASL) was observed from colloids created with other surfactants such as sodium dodecyl sulfate (SDS; anionic) and Pluronic F108 (nonionic) (see the Supporting Information).

Figure 2a illustrates the morphology evolution of a colloidal particle derived from a lamella-forming PS-b-P2VP block copolymer during the evaporation of chloroform. After emulsification, block copolymer chains are randomly distributed in the chloroform solution due to the low polymer concentration (1 wt %). As the solvent evaporates, the polymer concentration increases, and at a certain polymer concentration the still swollen block copolymers undergo microphase separation to form a lamellar structure inside the CTAB-coated emulsion droplet. Due to the fact that the interfacial energy of PS with the aliphatic tail of CTAB is lower than that of P2VP ($\gamma_{PS/CTAB} < \gamma_{P2VP/CTAB}$), the block copolymer colloidal particles formed an internal morphology consisting of radial lamellae with a PS wetting layer adjacent to the CTAB layer. Further evaporation of chloroform from the emulsion droplets results in
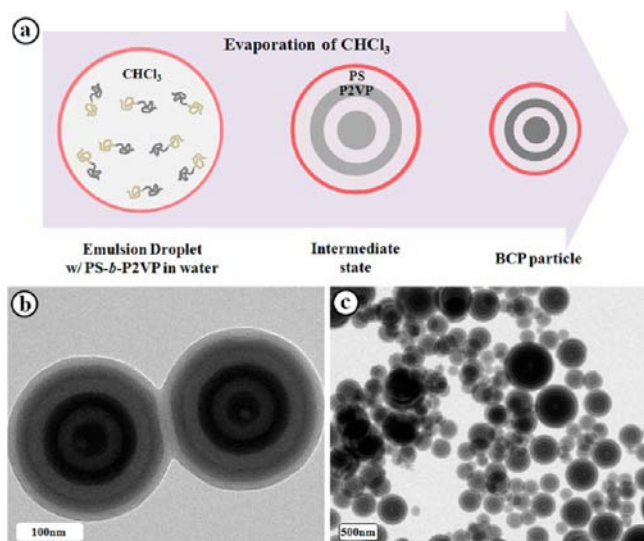
Figure 2. (a) Schematic illustration of PS-*b*-P2VP block copolymer self-assembly in a chloroform-in-water emulsion droplet that takes place during evaporation of chloroform. The concentration of block copolymer chains (1 wt %) increases during the evaporation of chloroform. At a certain concentration of block copolymer chains in chloroform, labeled "intermediate state", the chains self-assemble to an RL morphology due to preferential wetting of PS chains over P2VP on the aliphatic tail of CTAB (red circle) surrounding the spherical emulsion droplet. The formation of a PS layer at the intermediate state causes the final morphology of block copolymer colloidal particles to have the RL structure after complete evaporation of chloroform. (b, c) TEM images of spherical block copolymer colloidal particles with radial morphology. PS domains are gray shells, and P2VP domains appear as darker shells after staining with iodine vapor.

a decrease in the volume of the block copolymer colloidal particles, with the internal morphology being maintained due to the high glass transition temperatures for both blocks. Transmission electron microscopy (TEM) images in Figure 2b,c show the spherical block copolymer colloidal particles with a radial morphology. The PS and P2VP domains appear as light and dark gray shells, respectively, after staining with iodine vapor. In all cases, the outermost PS wetting layer exhibits a half-lamella thickness compared to the internal PS domains (Figure 2b). The size distribution of block copolymer colloidal particles is broad and ranges from several hundreds of nanometers to a few micrometers. This can be assigned to the emulsification method and the resulting polydispersity in the size of the initial emulsion droplets (Figure 2c).

To control the internal morphology of these colloidal particles, the preferential wetting of PS with the surrounding CTAB layer needs to be neutralized. In previous studies with thin films we have demonstrated the versatility of using SNPs to control such interfacial interactions in bulk lamella-forming PS-*b*-P2VP diblock copolymers, thereby inducing a morphology change to a disordered PS/P2VP bicontinuous morphology due to preferential nanoparticle segregation at the PS/P2VP interface.[27,28] By transferring this approach to a confined 3D droplet geometry, we found that the addition of these SNPs to a chloroform solution of PS-*b*-P2VP block copolymer dramatically changed the morphology of the resulting block copolymer colloidal particles from a traditional, spherical radial morphology to an ASL structure with an ellipsoidal shape (TEM micrograph in Figure 3b).

The power of using Au-based nanoparticles as interfacial agents is apparent as the internal morphology of the block copolymer colloidal particles and the distribution of SNPs could be characterized by tilted TEM micrographs (Figure 3c,d). It should be noted that alternating PS (lighter gray stripes) and P2VP (darker gray stripes) lamellar planes are clearly seen in the elongated ellipsoidal colloids in Figure 3c, with the SNPs being preferentially located at the three-phase (PS, P2VP, and surrounding CTAB) contact lines and at the P2VP/CTAB interfaces (outer surface of P2VP domain). This segregation of the SNPs into well-defined rings at the surface of the colloidal block copolymers can be seen in the tilted (30°) TEM micrograph in Figure 3d and could be further characterized by cross-sectional TEM micrographs (Figure 3e,f). Few SNPs were observed in the interior of the block copolymer colloidal particles as shown in the cross-sectional TEM micrographs that were sliced perpendicular (Figure 3e) and parallel (Figure 3f) to the lamellar planes, which illustrates the interfacial activity of these nanoparticles and their ability to control morphology. While not immediately apparent, the driving force for the attraction of the PS-coated Au NPs to the P2VP layers is the binding of the pyridyl groups to the surface of the Au NPs, which is still available for binding as the PS shell does not form a dense brush.

The ability of these Au-based SNPs to segregate specifically to P2VP interfaces was then examined for a much simpler system, i.e., colloidal particles formed from a blend of two homopolymers. Well-defined spherical "Janus" composite particles could be prepared by adding SNPs, with the volume fraction ϕ_p being ca. 4% of the total volume of PS and P2VP homopolymers (Figure 4). Significantly, the preferential adsorption of SNPs at both the P2VP/CTAB and the three-phase interfaces (SNP ring at the PS/P2VP interface) was again apparent from the TEM micrographs and allows composite Janus structures with a metal nanoparticle decorated hemisphere to be obtained in a single step. This ability to generate novel morphologies in multiple systems clearly demonstrates the versatility and potential of SNPs for controlling interfacial interactions in confined environments and supports the hypothesis that the mobility of SNPs at the emulsion/CTAB interface is critical for stabilization of these unique morphologies.

Apart from synthetic ease, another advantage of using SNPs to control interfacial interactions is the ability to tune those interactions by simply varying the nanoparticle loading.[57,58] To investigate this effect, block copolymer colloidal particles mixed with various feed volume fractions of SNPs (ϕ_p), ranging from 2.2% to 13.5%, were prepared, and the associated TEM micrographs are shown in the Supporting Information. Visually this can be best appreciated in Figure 5, which shows a representative image for particles obtained at low ϕ_p (2.2%) concentrations of SNPs. The shape of the block copolymer particles remained roughly spherical, indicating that the amount of SNPs was not enough to induce a morphology transition. However, the particles show a clear mixture of radial layers and axially stacked lamellae, with the SNPs being present at interfacial boundaries.

These experimental results provide clear evidence for the importance of SNPs in inducing a morphological transition of PS-*b*-P2VP block copolymer colloidal particles from "onion-like" spherical structures to ellipsoidal stacked lamellae. To understand the mechanism and driving force for this transformation, emulsion droplets dispersed in water were vitrified
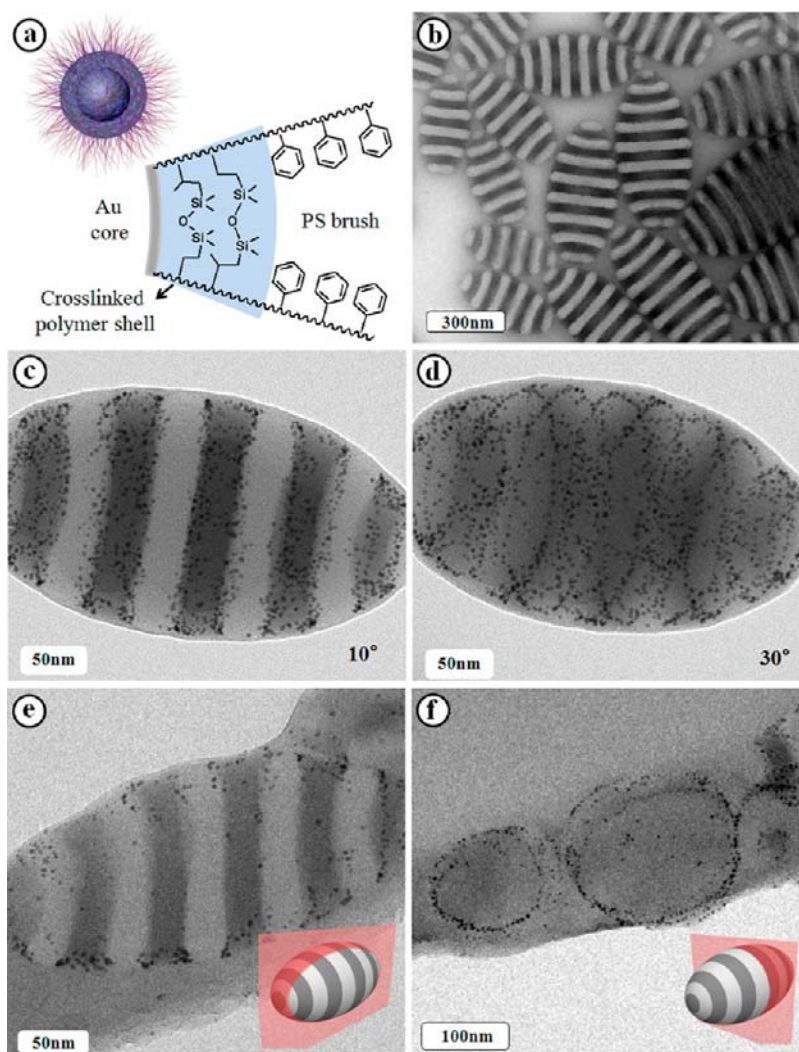
Figure 3. (a) Structural illustration of an SNP. The SNP has a core–shell structure with the gold core surrounded by a cross-linked polyisoprene inner shell (containing Pt from the hydrosilation catalyst)[27] and a PS outer brush. (b) TEM micrograph of block copolymer colloidal particles with ASL morphology obtained by addition of SNPs to a chloroform solution of block copolymer. The other experimental conditions were the same as in the production of block copolymer colloidal particles with the RL structure in Figure 2. The feed volume fraction of SNPs (ϕ_p) was 14%. Light gray stripes are PS domains, and dark gray stripes are P2VP domains after staining with iodine vapor. (c, d) TEM micrographs of a block copolymer colloidal particle tilted at angles of 10° and 30°. The SNPs were preferentially segregated along the three-phase interface of PS, P2VP, and the surrounding CTAB, with a significant concentration at the P2VP/CTAB interface. (e, f) Cross-sectional TEM images of block copolymer colloidal particles sliced perpendicular and parallel, respectively, to the lamellar planes.

with liquid ethane and characterized using cryo-TEM before complete evaporation of the chloroform (Figure 6a,b). In Figure 6a, the initial chloroform emulsion droplet has a spherical shape and contains randomly organized SNPs with no observable block copolymer phase separation. In contrast to Figure 2a, as the chloroform evaporates, segregation of SNPs at the three-phase and the P2VP/CTAB interfaces occurs, resulting in formation of PS-b-P2VP colloidal particles with ellipsoid shape and stacked lamellar morphology. During (or after) emulsification, the SNPs, which were initially dispersed in chloroform, migrate and adsorb to the emulsion/CTAB (red circle) interface as observed from cryo-TEM experiments. The SNPs are then mobile at the emulsion/CTAB interface and rearrange their locations during the intermediate stages of microphase separation and particle formation. In contrast to the preferential wetting of PS domains on the emulsion/CTAB interface (left illustration in Figure 6d), the "favorable interaction" between the SNPs and P2VP chains allows the

P2VP domains to be exposed to the emulsion/CTAB interface together with PS domains, resulting in a lamellar structure (right illustration in Figure 6d). After further evaporation of chloroform, the emulsion droplet further decreases in size and transforms into a prolate ellipsoidal shape. Preliminary small-angle X-ray scattering (SAXS) experiments support this evolution pathway.

As can be seen in Figure 7a, for $\phi_p \approx 14\%$, the density of SNPs was sufficiently high to fully neutralize the interaction between PS-b-P2VP and CTAB such that the ASL morphology was formed at all particle sizes. Interestingly, a dependency of the shape anisotropy of the block copolymer colloidal particles on their respective sizes was observed and is further discussed in the Supporting Information. While this effect is plotted in Figure 7b as the aspect ratio L/S vs L (L and S are the lengths of the long and short axes of the ellipsoidal block copolymer colloidal particles, respectively), the physical principle that
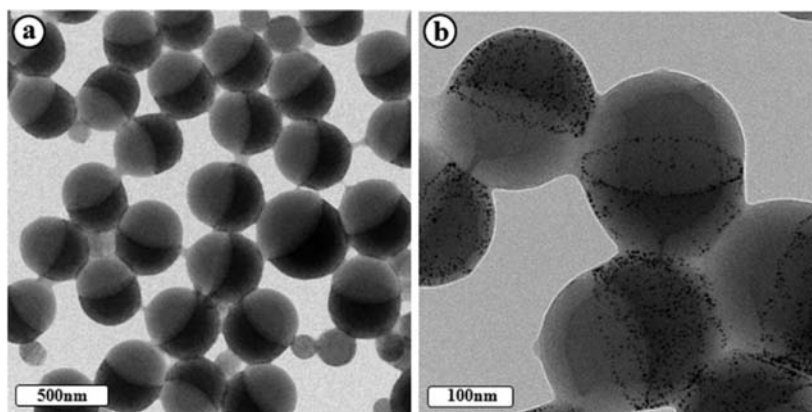
Figure 4. TEM micrographs of Janus colloidal particles created by emulsion synthesis using PS (100 kg/mol) and P2VP (100 kg/mol) homopolymers mixed with SNPs ($\phi_p \approx 4\%$ of the total volume of PS and P2VP homopolymers) in chloroform. The lighter gray hemisphere is PS, and the darker gray one is P2VP stained with iodine. Adsorption of the SNPs at the P2VP/CTAB interface indicated that the SNPs had a more attractive interaction with P2VP than PS chains. In addition, segregation of the SNPs at the three-phase interface (PS, P2VP, and surrounding CTAB) was observed as the formation of a necklace along the equators of Janus colloidal particles.
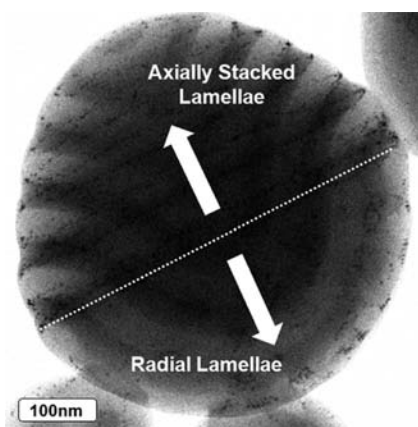

Figure 5. TEM micrograph of a representative PS-*b*-P2VP block copolymer colloidal particle showing mixed morphologies—radial and stacked lamellae induced by the addition of SNPs. The feed volume fraction of SNPs (ϕ_p) was 2.2%.

dictates this anisotropy versus size dependence of the ASL colloidal particles is not known.

In an attempt to explain these observations, a proposed theoretical explanation for breaking of spherical symmetry and particle elongation was developed. Two separate equilibrium mechanisms for driving the droplet shape toward a prolate ellipsoid can be proposed: (i) anisotropy of the interfacial tension between the block copolymer droplet and the surrounding CTAB/SNP interface and (ii) commensurability effects associated with the preferred lamellar spacing of the confined block copolymer droplet.

In evaluating interfacial tension anisotropy as a possible mechanism, SCFT simulations were performed on a symmetric, lamellar AB block copolymer against an incompatible C homopolymer in both parallel (lamellar normal in the direction of the AB/C interface normal) and perpendicular (lamellar normal perpendicular to the interface normal) configurations. While the simulations revealed a weak energetic preference for the perpendicular configuration, which favors prolate ellipsoidal droplets according to the Wulff construction,[59,60] the interfacial tension anisotropy was insufficient to produce an aspect ratio L/S greater than 1.05 for a range of $\chi_{AB}N$, $\chi_{AC}N$, and $\chi_{BC}N$. This is in direct contrast to the experimental aspect ratios

shown in Figure 7b, which were all significantly greater than the maximum predicted value of 1.05.

The role of commensurability between the lamellar spacing and the finite droplet size—in effect a bulk elasticity effect—was then investigated as a possible mechanism. This phenomenon has been well studied in block copolymer thin films, due to both vertical and lateral confinement,[61−63] but has not been explored in any detail in the context of 3D confinement created by the free surface of an emulsion drop. To this end, a simple theoretical model was developed that assumes strong segregation of the block copolymer, an assumption validated by our estimate of $\chi_{AB}N = \chi_{PS/P2VP}N = 200$ (see the Supporting Information for justification). The expression for the free energy is composed of three parts: a stretching penalty term for PS-*b*-P2VP, the interfacial energy between PS and P2VP, and the interfacial energy between PS-*b*-P2VP and the surrounding medium. For the stretching term, a standard entropic spring was adopted,[64] and for the energy of the interface between PS and P2VP, the surface tension of PS and P2VP, estimated from the results of Helfand and Tagami,[65] was multiplied by the total interfacial area of PS and P2VP. Finally, for the energy of the interface between PS-*b*-P2VP and the surrounding medium, the surface tension between PS-*b*-P2VP and the surrounding medium was multiplied by the total surface area of the ellipsoid.

Since the surface tension between PS-*b*-P2VP and the surrounding medium as a function of the areal density of SNPs (Σ) was unknown, we chose a functional form that monotonically decreases with increasing areal density and asymptotes to zero. To describe the droplet surface tension, the following formula was used:

$$\gamma = \frac{\gamma_0}{(1 + \Sigma/\Sigma_0)^\alpha}$$

where γ_0 is the surface tension between PS-*b*-P2VP and CTAB in water, Σ is the areal density of SNPs, and Σ_0 and α are fitting parameters. If the PS-*b*-P2VP and SNPs in different droplets cannot exchange, the SNPs are localized at the droplet interfaces, and the chloroform concentration is identical in all of the colloidal particles when they become glassy, the areal density Σ can be written as the number density of SNPs (ρ_{SNP}) in the particles when they became glassy times the volume of
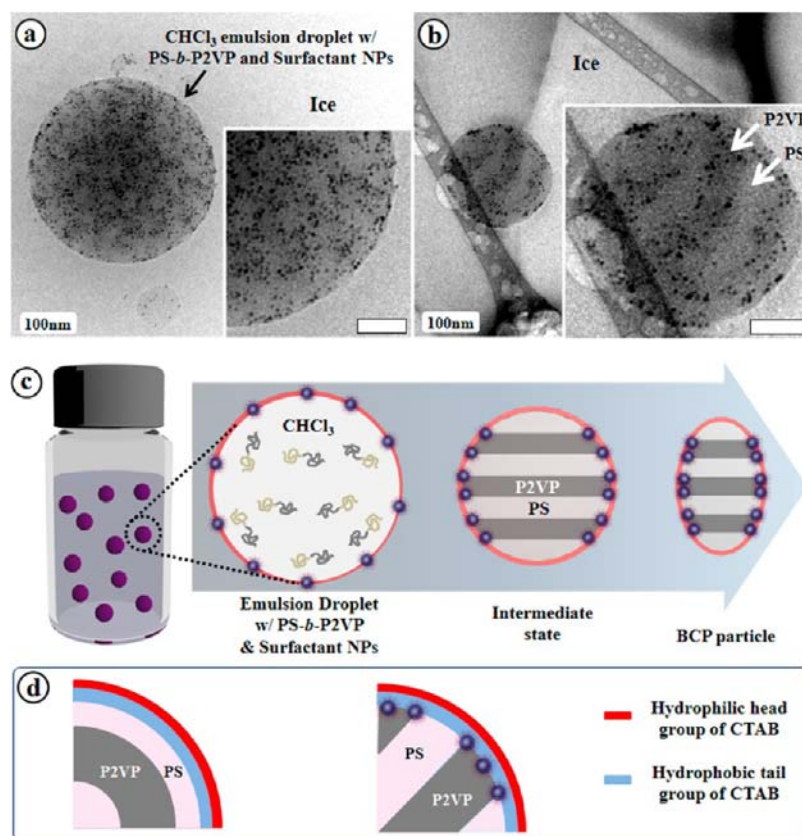
Figure 6. (a) Cryo-TEM micrograph of a vitrified emulsion droplet in water. The SNPs, shown as black dots, surrounding the emulsion droplet are randomly distributed at the emulsion/CTAB interface. (b) Cryo-TEM micrograph of an emulsion droplet at (or after) the intermediate state. The feed volume fraction of SNPs (ϕ_p) in PS-b-P2VP block copolymer was 14% for both images. Scale bars in the insets are 50 nm. (c) Schematic illustrating the formation mechanism of the PS-b-P2VP colloidal particles with ASL structure from an emulsion droplet of chloroform. In contrast to the preferential wetting of PS domains on the emulsion/CTAB interface (d, left), favorable interaction between the SNPs and P2VP chains results in an ASL structure (d, right).
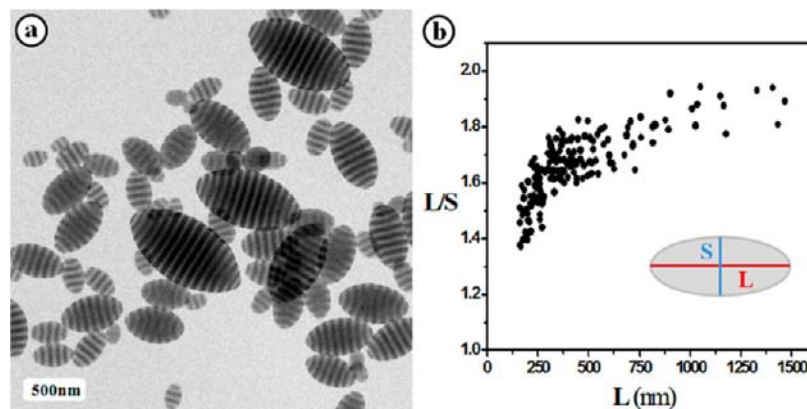

Figure 7. (a) TEM micrographs of polydisperse PS-b-P2VP block copolymer colloidal particles mixed with SNPs at a feed volume fraction of ∼14% and (b) their shape anisotropy related to particle size, i.e., L/S vs S, where L and S are the lengths of the long and short axes, respectively.

the ellipsoid divided by the surface area of the ellipsoid. Since an explicit number for the density of SNPs is unknown, we can combine it with the fitting parameter Σ_0 to form a new fitting parameter (ρ_{SNP}/Σ_0).

Additionally, to keep the theory simple, we have assumed idealized geometries, namely, droplets that are prolate ellipsoids with flat PS/P2VP interfaces, and that the particles contain only an even number of layers since the mass balance of PS and P2VP is then automatically satisfied. Although odd numbers of

layers will not be predicted, the resulting trend should be unaffected.

To calculate the anisotropy of the ASL colloidal particles for a given set of fitting parameters, the free energy was minimized with respect to the aspect ratio and number of layers of lamellae for fixed colloidal particle volumes. Herein, the complete expression for the free energy of the colloidal particle is a function of the number of layers of lamellae inside the particle (n), the aspect ratio of the ellipsoid (L/S), and the volume of the ellipsoid (V) (see the Supporting Information for details).

In addition, it was assumed that the volumes of the particles were fixed from the sonication procedure; i.e., coalescence or ripening effects were negligible.

To validate the model, we have compared its predictions to SCFT simulations of a block copolymer droplet in an immiscible environment at low $\chi_{AB}N$ and for small particles due to the numerical cost of the simulations. We found that the SCFT simulations exhibit trends similar to those of the theory. The fitting parameters in our theory were determined from a least-squares minimization procedure outlined in the Supporting Information. With this procedure, the two fit parameters are α = 1.3 and ρ_{SNP}/Σ_0 = 1.1 nm^{-1}. The resulting theoretical prediction along with the experimental data from Figure 7b can be seen in Figure 8. As the size L of the colloidal particle
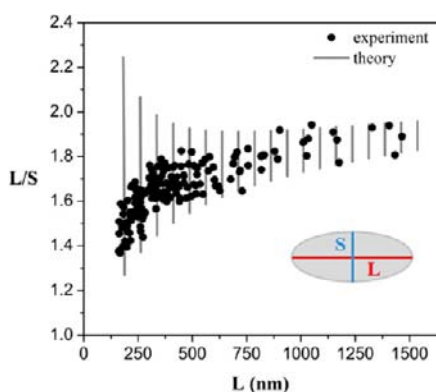

Figure 8. Aspect ratio as a function of size for PS-*b*-P2VP block copolymer colloidal particles mixed with an SNP feed volume fraction of ~14% determined from TEM micrographs and predicted from a theoretical model. The particle anisotropy is plotted as L/S vs S, where L and S are the lengths of the long and short axes, respectively. Each theoretical line corresponds to a different number of layers in the particle.

increases, the particle elongates until L is an integral multiple of the block copolymer period L_0, at which point another two layers of PS-*b*-P2VP are added and the aspect ratio L/S discontinuously drops to a smaller value. Thus, each theoretical branch corresponds to a different number of layers in the colloidal particle, and the top and bottom envelopes of the various branches put bounds on the range of aspect ratios L/S that would be expected at each particle size L. These theoretical branches only appear to be vertical due to the compressed x axis in Figure 8. Note that the overprediction of the aspect ratio for smaller colloidal particles corresponds to the region where the diblock layers are under the most compression as compared to the bulk layer spacing. Thus, it is likely that by accounting for odd number of layers or curved interfaces, the overprediction would be reduced. Nonetheless, the salient features of the experimental data were captured by the theoretical model. This suggests that the size distribution of the colloidal particles with a sufficient number of SNPs to neutralize the P2VP and form an ASL structure can be described purely by the competition of polymer chain stretching, copolymer PS/P2VP interfacial interactions, and a reduction of the surface tension of PS-*b*-P2VP against the surrounding medium upon localizing increasing numbers of available SNPs (larger L implies more particles) to the droplet interface. Thus, thermodynamic factors appear to be controlling particle anisotropy in the limit of a sufficient number of SNPs. Ultimately, the theoretical model

can be used to tune the existing system or aid the design of new anisotropic colloids. Reducing the polymer molecular weight lowers the elastic strain contribution to the free energy and reduces the domain spacing in the colloidal particles while leaving the external surface tension contribution unaffected. Consequently, the aspect ratios achieved should also be reduced. The inverse is expected for increased molecular weight. Another way to tune the system is to modify the SNP concentration, which enters the model only through the combination parameter ρ_{SNP}/Σ_0. Increased SNP concentration lowers the external surface tension and should result in more elongated colloidal particles. Additionally, adjusting the surface treatment of the SNPs could have consequences for their activity at the colloid interface. With this understanding, the model could be used to anticipate the colloid shape.

■ CONCLUSIONS

A simple, yet powerful strategy for controlling nanoscale morphology in the confined geometry of colloidal particles based on the use of SNPs has been developed. Addition of SNPs to colloidal particles containing lamella-forming PS-*b*-P2VP diblock copolymers results in a dramatic transition from a traditional spherical, radial morphology to unique axially stacked lamella ellipsoids. Significantly, it was observed that the SNPs preferentially adsorb at the emulsion interface and modify the interfacial interactions between block copolymer domains, leading to a neutral wetting of PS and P2VP lamellae at the particle surface. Similar behavior was also observed for colloidal particles formed from a blend of PS and P2VP homopolymers, where well-defined Janus particles could be obtained and stabilized by preferential segregation of the SNPs to both the external PS/P2VP interface and the P2VP hemisphere. To understand the assembly of these multicomponent materials, a simple free energy model that embodies the competition between SNP-mediated particle/medium surface tension and smectic elasticity, namely, commensurability of the lamellar stacks with the long axis of the colloidal particle, was developed. This model accurately describes the aspect ratio of these anisotropic block copolymer colloidal particles as a function of particle size. Future work will address the creation of nonconventional composite colloidal particles with multifunctionality and complex hierarchical structures.

■ EXPERIMENTAL SECTION

Synthesis of Surfactant Nanoparticles. SNPs were synthesized by previously reported methods[27,28] and based on Au nanoparticles coated with PS-*b*-PI-SH ligands (PS-*b*-PI-SAu). The thiol-terminated poly(styrene-*b*-1,2- and 3,4-isoprene) (PS-*b*-PI-SH) ligands were synthesized by sequential anionic polymerization using tetrahydrofuran (THF) as a solvent at −78 °C with number average molar mass (M_n) values of the PS block of 3 kg/mol and the PI block of 1.4 kg/mol.

Synthesis of PS-*b*-P2VP Block Copolymer Colloidal Particles. Block copolymer colloidal particles were created by an emulsification strategy involving dissolution of PS-*b*-P2VP block copolymer (199 kg/mol, Polymer Source Inc.) in 2 mL of chloroform (1 wt %). This block copolymer solution was emulsified by ultrasonication in 15 mL of deionized water containing CTAB (Sigma-Aldrich, 0.1 wt %) as a surfactant. Then the emulsion was poured into a 100 mL beaker containing an aqueous CTAB solution (0.1 wt %, 10 mL) and stirred for 1 day (100 rpm). To allow chloroform to slowly evaporate, the beaker was covered with a glass lid. After complete evaporation of chloroform, the solid block copolymer colloidal particles were washed

by centrifugation at 10 000 rpm for 10 min followed by redispersion in deionized water.

Characterization. Images of the block copolymer colloidal particles and their cross sections were taken by TEM (FEI Tecnai G2 microscope, 200 kV). The block copolymer nanoparticle samples were prepared on carbon-coated TEM grids by drop casting the aqueous block copolymer nanoparticle dispersion. For cross-sectional TEM micrographs, aqueous dispersions of block copolymer colloidal particles were drop cast on precured epoxy resin (Embed-812, Electron Microscopy Sciences). After evaporation of water, the epoxy resin with block copolymer colloidal particles was embedded into additional epoxy resin on top. Then the cured resin (60 °C for 12 h) was sliced to a thickness of about 100 nm by ultramicrotoming (Leica). The samples for cryogenic transmission electron microscopy (cryo-TEM) were prepared by pipetting a 3.5 mL droplet of emulsion onto a glow-discharged lacey carbon coated copper grid. The samples were vitrified in liquid nitrogen cooled liquid ethane using the environmentally controlled FEI Vitrobot Mark IV (24 °C, 100% humidity). After vitrification, the grid was placed in a Gatan cryoholder and was kept below −165 °C throughout imaging. Imaging was performed using low-dose mode, and the images were recorded digitally with a Gatan Ultrascan 1000 CCD camera and analyzed using the Gatan Digital Micrograph software.

ASSOCIATED CONTENT

ⓢ Supporting Information

Synthesis and characterization of the nanoparticles/composite systems and the development of the theoretical model and simulations. This material is available free of charge via the Internet at http://pubs.acs.org

AUTHOR INFORMATION

Corresponding Author

ghf@mrl.ucsb.edu; edkramer@mrl.ucsb.edu; hawker@mrl.ucsb.edu

Present Address

∇S.G.J.: Korea Electric Power Research Institute, Daejeon 305-701, Republic of Korea.

Notes

The authors declare no competing financial interest.

ACKNOWLEDGMENTS

REFERENCES

(1) Bockstaller, M. R.; Thomas, E. L. *J. Phys. Chem. B* **2003**, *107*, 10017−10024.

(2) Elsabahy, M.; Wooley, K. L. *J. Polym. Sci., Part A: Polym. Chem.* **2012**, *50*, 1869−1880.

(3) Jaramillo, T. F.; Baeck, S. H.; Cuenya, B. R.; McFarland, E. W. *J. Am. Chem. Soc.* **2003**, *125*, 7148−7149.

(4) Keng, P. Y.; Bull, M. M.; Shim, I. B.; Nebesny, K. G.; Armstrong, N. R.; Sung, Y.; Char, K.; Pyun, J. *Chem. Mater.* **2011**, *23*, 1120−1129.

(5) (a) Grubbs, R. B. *Nat. Mater.* **2007**, *6*, 553−555. Pochan, D. J.; Zhu, J.; Zhang, K.; Wooley, K. L.; Miesch, C.; Emrick, T. *Soft Matter* **2011**, *7*, 2500−2506. (c) Pan, Q.; Tong, C.; Zhu, Y. *ACS Nano* **2011**,

(5) 123−128. (d) Li, Z.; Sai, H.; Warren, S. C.; Kamperman, M.; Arora, H.; Gruner, S. M.; Wiesner, U. *Chem. Mater.* **2009**, *21*, 5578−5584. (e) Rasch, M. R.; Rossinyol, E.; Hueso, J. L.; Goodfellow, B. W.; Arbiol, J.; Korgel, B. A. *Nano Lett.* **2010**, *10*, 3733−3739. (f) Moughton, A. O.; Hillmyer, M. A.; Lodge, T. P. *Macromolecules* **2012**, *45*, 2−19.

(6) Lee, S. W.; Kumpfer, J. R.; Lin, P. A.; Li, G. D.; Gao, X. P. A.; Rowan, S. J.; Sankaran, R. M. *Macromolecules* **2012**, *45*, 8201−8210.

(7) Chiu, J. J.; Kim, B. J.; Kramer, E. J.; Pine, D. J. *J. Am. Chem. Soc.* **2005**, *127*, 5036−5037.

(8) Chiu, J. J.; Kim, B. J.; Yi, G. R.; Bang, J.; Kramer, E. J.; Pine, D. J. *Macromolecules* **2007**, *40*, 3361−3365.

(9) Chung, H.; Ohno, K.; Fukuda, T.; Composto, R. J. *Nano Lett.* **2005**, *5*, 1878−1882.

(10) Hickey, R. J.; Sanchez-Gaytan, B. L.; Cui, W. H.; Composto, R. J.; Fryd, M.; Wayland, B. B.; Park, S. J. *Small* **2010**, *6*, 48−51.

(11) Costanzo, P. J.; Beyer, F. L. *Macromolecules* **2007**, *40*, 3996−4001.

(12) Kang, H.; Detcheverry, F. A.; Mangham, A. N.; Stoykovich, M. P.; Daoulas, K. C.; Hamers, R. J.; Muller, M.; de Pablo, J. J.; Nealey, P. F. *Phys. Rev. Lett.* **2008**, *100*, 148303.

(13) Kim, B. J.; Bang, J.; Hawker, C. J.; Chiu, J. J.; Pine, D. J.; Jang, S. G.; Yang, S. M.; Kramer, E. J. *Langmuir* **2007**, *23*, 12693−12703.

(14) Kim, B. J.; Bang, J.; Hawker, C. J.; Kramer, E. J. *Macromolecules* **2006**, *39*, 4108−4114.

(15) Kim, B. J.; Fredrickson, G. H.; Hawker, C. J.; Kramer, E. J. *Langmuir* **2007**, *23*, 7804−7809.

(16) Kim, B. J.; Fredrickson, G. H.; Kramer, E. J. *Macromolecules* **2008**, *41*, 436−447.

(17) Böker, A.; Lin, Y.; Chiapperini, K.; Horowitz, R.; Thompson, M.; Carreon, V.; Xu, T.; Abetz, C.; Skaff, H.; Dinsmore, A. D.; Emrick, T.; Russell, T. P. *Nat. Mater.* **2004**, *3*, 302−306.

(18) Hu, Y. X.; Chen, D. A.; Park, S.; Emrick, T.; Russell, T. P. *Adv. Mater.* **2010**, *22*, 2583−2587.

(19) Jang, S. G.; Kramer, E. J.; Hawker, C. J. *J. Am. Chem. Soc.* **2010**, *133*, 16986−16996.

(20) Jang, S. G.; Khan, A.; Hawker, C. J.; Kramer, E. J. *Macromolecules* **2012**, *45*, 1553−1561.

(21) Li, Q. F.; He, J. B.; Glogowski, E.; Li, X. F.; Wang, J.; Emrick, T.; Russell, T. P. *Adv. Mater.* **2008**, *20*, 1462−1466.

(22) Lin, Y.; Daga, V. K.; Anderson, E. R.; Gido, S. P.; Watkins, J. J. *J. Am. Chem. Soc.* **2011**, *133*, 6513−6516.

(23) Yeh, S. W.; Chang, Y. T.; Chou, C. H.; Wei, K. H. *Macromol. Rapid Commun.* **2004**, *25*, 1680−1686.

(24) Yeh, S. W.; Wei, K. H.; Sun, Y. S.; Jeng, U. S.; Liang, K. S. *Macromolecules* **2003**, *36*, 7903−7907.

(25) Kim, B. J.; Chiu, J. J.; Yi, G. R.; Pine, D. J.; Kramer, E. J. *Adv. Mater.* **2005**, *17*, 2618−2622.

(26) Kim, B. J.; Fredrickson, G. H.; Bang, J.; Hawker, C. J.; Kramer, E. J. *Macromolecules* **2009**, *42*, 6193−6201.

(27) Jang, S. G.; Dimitriou, M. D.; Kim, B. J.; Lynd, N. A.; Kramer, E. J.; Hawker, C. J. *Soft Matter* **2011**, *7*, 6255−6263.

(28) Jang, S. G.; Kim, B. J.; Hawker, C. J.; Kramer, E. J. *Macromolecules* **2011**, *44*, 9366−9373.

(29) (a) Lee, J. Y.; Shou, Z. Y.; Balazs, A. C. *Macromolecules* **2003**, *36*, 7730−7739. (b) Frischknecht, A. L.; Padmanabhan, V.; Mackay, M. E. *J. Chem. Phys.* **2012**, *136*, 164904.

(30) Yoo, M.; Kim, S.; Jang, S. G.; Choi, S. H.; Yang, H.; Kramer, E. J.; Lee, W. B.; Kim, B. J.; Bang, J. *Macromolecules* **2011**, *44*, 9356−9365.

(31) Park, S. C.; Kim, B. J.; Hawker, C. J.; Kramer, E. J.; Bang, J.; Ha, J. S. *Macromolecules* **2007**, *40*, 8119−8124.

(32) Lin, Y.; Boker, A.; He, J. B.; Sill, K.; Xiang, H. Q.; Abetz, C.; Li, X. F.; Wang, J.; Emrick, T.; Long, S.; Wang, Q.; Balazs, A.; Russell, T. P. *Nature* **2005**, *434*, 55−59.

(33) Chen, J. T.; Zhang, M. F.; Yang, L.; Collins, M.; Parks, J.; Avallone, A.; Russell, T. P. *J. Polym. Sci., Part B: Polym. Phys.* **2007**, *45*, 2912−2917.

(34) Sun, Y. M.; Steinhart, M.; Zschech, D.; Adhikari, R.; Michler, G. H.; Gosele, U. *Macromol. Rapid Commun.* **2005**, *26*, 369−375.

(35) Xiang, H. Q.; Shin, K.; Kim, T.; Moon, S. I.; McCarthy, T. J.; Russell, T. P. *Macromolecules* **2004**, *37*, 5660−5664.

(36) Cheng, J. Y.; Ross, C. A.; Smith, H. I.; Thomas, E. L. *Adv. Mater.* **2006**, *18*, 2505−2521.

(37) Wu, Y. Y.; Cheng, G. S.; Katsov, K.; Sides, S. W.; Wang, J. F.; Tang, J.; Fredrickson, G. H.; Moskovits, M.; Stucky, G. D. *Nat. Mater.* **2004**, *3*, 816−822.

(38) Yabu, H.; Jinno, T.; Koike, K.; Higuchi, T.; Shimomura, M. *J. Polym. Sci., Part B: Polym. Phys.* **2011**, *49*, 1717−1722.

(39) Pinna, M.; Hiltl, S.; Guo, X. H.; Boker, A.; Zvelindovsky, A. V. *ACS Nano* **2010**, *4*, 2845−2855.

(40) Chi, P.; Wang, Z.; Li, B. H.; Shi, A. C. *Langmuir* **2011**, *27*, 11683−11689.

(41) Yabu, H.; Koike, K.; Motoyoshi, K.; Higuchi, T.; Shimomura, M. *Macromol. Rapid Commun.* **2010**, *31*, 1267−1271.

(42) Higuchi, T.; Motoyoshi, K.; Sugimori, H.; Jinnai, H.; Yabu, H.; Shimomura, M. *Macromol. Rapid Commun.* **2010**, *31*, 1773−1778.

(43) Higuchi, T.; Tajima, A.; Motoyoshi, K.; Yabu, H.; Shimomura, M. *Angew. Chem., Int. Ed.* **2009**, *48*, 5125−5128.

(44) Higuchi, T.; Tajima, A.; Motoyoshi, K.; Yabu, H.; Shimomura, M. *Angew. Chem., Int. Ed.* **2008**, *47*, 8044−8046.

(45) Yabu, H.; Motoyoshi, K.; Higuchi, T.; Shimomura, M. *Phys. Chem. Chem. Phys.* **2010**, *12*, 11944−11947.

(46) Li, L.; Matsunaga, K.; Zhu, J. T.; Higuchi, T.; Yabu, H.; Shimomura, M.; Jinnai, H.; Hayward, R. C.; Russell, T. P. *Macromolecules* **2010**, *43*, 7807−7812.

(47) Higuchi, T.; Tajima, A.; Yabu, H.; Shimomura, M. *Soft Matter* **2008**, *4*, 1302−1305.

(48) Jeon, S. J.; Yi, G. R.; Yang, S. M. *Adv. Mater.* **2008**, *20*, 4103−4108.

(49) Jeon, S. J.; Yi, G. R.; Koo, C. M.; Yang, S. M. *Macromolecules* **2007**, *40*, 8430−8439.

(50) Glotzer, S. C.; Solomon, M. J. *Nat. Mater.* **2007**, *6*, 557−562.

(51) (a) Fejer, S. N.; Chakrabarti, D.; Wales, D. J. *Soft Matter* **2011**, *7*, 3553−3564. (b) Hawker, C. J.; Saville, P. M.; White, J. W. *J. Org. Chem.* **1994**, *59*, 3503−3505.

(52) Lele, P. P.; Furst, E. M. *Langmuir* **2009**, *25*, 8875−8878.

(53) Lu, Y.; Yin, Y. D.; Li, Z. Y.; Xia, Y. N. *Langmuir* **2002**, *18*, 7722−7727.

(54) Doshi, N.; Mitragotri, S. *J. R. Soc., Interface* **2010**, *7*, S403−S410.

(55) Champion, J. A.; Katare, Y. K.; Mitragotri, S. *Proc. Natl. Acad. Sci. U.S.A.* **2007**, *104*, 11901−11904.

(56) Yoo, J. W.; Mitragotri, S. *Proc. Natl. Acad. Sci. U.S.A.* **2010**, *107*, 11205−11210.

(57) Connal, L. A.; Lynd, N. A.; Robb, M. J.; See, K. A.; Jang, S. G.; Spruell, J. M.; Hawker, C. J. *Chem. Mater.* **2012**, *24*, 4036−4042.

(58) Robb, M. J.; Connal, L. A.; Lee, B. F.; Lynd, N. A.; Hawker, C. J. *Polym. Chem.* **2012**, *3*, 1618−1628.

(59) Balsara, N. P.; Marques, C. M.; Garetz, B. A.; Newstein, M. C.; Gido, S. P. *Phys. Rev. E* **2002**, *66*, 052802−1:4.

(60) Chaikin, P. M.; Lubensky, T. C. *Principals of Condensed Matter Physics*; Cambridge University Press: Cambridge, U.K., 1995.

(61) Matsen, M. W. *J. Chem. Phys.* **1997**, *106*, 7781−7791.

(62) Bosse, A. W.; García-Cervera, C. J.; Fredrickson, G. H. *Macromolecules* **2007**, *40*, 9570−9581.

(63) Hur, S.-M.; García-Cervera, C. J.; Kramer, E. J.; Fredrickson, G. H. *Macromolecules* **2009**, *42*, 5861−5872.

(64) Bates, F. S.; Fredrickson, G. H. *Phys. Today* **1999**, *52*, 32−38.

(65) Helfand, E.; Tagami, Y. *J. Polym. Sci., Part B: Polym. Lett.* **1971**, *9*, 741−746.